ONCOIMMUNOLOGY
2023, VOL. 12, NO. 1, 2158610
https://doi.org/10.1080/2162402X.2022.2158610

Taylor & Francis
Taylor & Francis Group

ORIGINAL RESEARCH

OPEN ACCESS Check for updates

# Thiopurine 6TG treatment increases tumor immunogenicity and response to immune checkpoint blockade

Loulieta Nazerai[a,b], Shona Caroline Willis[a,b], Patricio Yankilevich[c], Luca Di Leo[a], Francesca Maria Bosisio[d], Alex Frias[a], Corine Bertolotto[e,f], Jacob Nersting[b], Maria Thastrup[b], Soren Buus[g], Allan Randrup Thomsen[g], Morten Nielsen[h], Kristoffer Staal Rohrberg[i], Kjeld Schmiegelow[b#], and Daniela De Zio[a,j#]

[a]Melanoma Research Team, Danish Cancer Society Research Center, Copenhagen, Denmark; [b]Department of Pediatrics and Adolescent Medicine, Rigshospitalet, University of Copenhagen, Copenhagen, Denmark; [c]Bioinformatics Core Facility, Instituto de Investigación En Biomedicina de Buenos Aires (Ibioba), Buenos Aires, Argentina; [d]Lab of Translational Cell and Tissue Research, University of Leuven, Leuven, Belgium; [e]Universite Côte d'Azur, Nice, France; [f]INSERM, Biology and Pathologies of melanocytes, team1, Equipe labellisée Ligue 2020, Centre Méditerranéen de Médecine Moléculaire, Nice, France; [g]Department of Immunology and Microbiology, University of Copenhagen, Copenhagen, Denmark; [h]Department of Health Technology, Section for Bioinformatics, Technical University of Denmark, Lyngby, Denmark; [i]Department of Oncology, Rigshospitalet, University of Copenhagen, Copenhagen, Denmark; [j]Department of Drug Design and Pharmacology, University of Copenhagen, Copenhagen, Denmark

**ABSTRACT**

Immune-checkpoint inhibitors (ICI) are highly effective in reinvigorating T cells to attack cancer. Nevertheless, a large subset of patients fails to benefit from ICI, partly due to lack of the cancer neoepitopes necessary to trigger an immune response. In this study, we used the thiopurine 6-thioguanine (6TG) to induce random mutations and thus increase the level of neoepitopes presented by tumor cells. Thiopurines are prodrugs which are converted into thioguanine nucleotides that are incorporated into DNA (DNA-TG), where they can induce mutation through single nucleotide mismatching. In a pre-clinical mouse model of a mutation-low melanoma cell line, we demonstrated that 6TG induced clinical-grade DNA-TG integration resulting in an improved tumor control that was strongly T cell dependent. 6TG exposure increased the tumor mutational burden, without affecting tumor cell proliferation and cell death. Moreover, 6TG treatment re-shaped the tumor microenvironment by increasing T and NK immune cells, making the tumors more responsive to immune-checkpoint blockade. We further validated that 6TG exposure improved tumor control in additional mouse models of melanoma. These findings have paved the way for a phase I/II clinical trial that explores whether treatment with thiopurines can increase the proportion of otherwise treatment-resistant cancer patients who may benefit from ICI therapy (NCT05276284).

**ARTICLE HISTORY**
Received 1 September 2022
Revised 8 December 2022
Accepted 9 December 2022

**KEYWORDS**
Thiopurine; 6TG; immune checkpoint inhibitors; melanoma; mouse model

## Introduction

Antitumor immune responses are dependent on the activation of T cells [CD8 cytotoxic T lymphocytes and CD4 T helper cells (*e.g.*, Th1, Th17)][1,2] to efficiently kill cancer cells that present neoepitopes induced by their acquired mutations. Many cancers can avoid such immune responses by the expression of ligands to inhibitory receptors on the recruited T-cells,[3] such as Programmed cell death protein 1 (PD-1) and cytotoxic T-lymphocyte-associated antigen 4 (CTLA-4). Thus, a novel strategy for treating cancer is the use of immune-checkpoint inhibitors (ICI), which block the interaction between the inhibitory receptors on T cells with their ligand on cancer cells and professional antigen presenting cells, thus (re)activating T cells to attack and eliminate malignant cells.[3] The use of ICI has revolutionized the treatment of several otherwise treatment-resistant cancers, but most patients fail to obtain durable or even any responses as many cancer types are resistant to ICI therapy.[4,5] Pre-clinical studies have pointed to the paucity of tumor neoantigens as a bottleneck for efficiency of check point inhibition.[6] Notably, mutations acquired during tumorigenesis can increase the number of neoepitopes on tumor cells and elicit cytotoxic T-cell responses, which can be enhanced by ICI therapy.[7,8] Accordingly, tumor mutational burden (TMB), which is defined as the number of somatic non-synonymous mutations per megabase (mut/Mb) of coding regions of a tumor genome, has emerged as a predictor of responses to ICI therapy for several cancers.[9–12]

The thiopurines 6-mercaptopurine (6MP) and 6-thioguanine (6TG) have for decades been used in the treatment of hematological cancers. Thiopurines are converted into thioguanine nucleotides (TGN), which are then incorporated into DNA (DNA-TG) in competition with normal guanine.[13] Random methylation of DNA-TG favors fraudulent G·T mismatching which leads to either apoptosis after futile mismatch repair (MMR) attempts or novel mutations. In a clinical trial, higher DNA-TG levels during 6MP maintenance therapy of acute lymphoblastic leukemia (ALL) patients were correlated with reduced relapse risks,[14,15] which could reflect higher

**CONTACT** Daniela De Zio dzio@cancer.dk Melanoma Research Team, Danish Cancer Society Research Center, Copenhagen, Denmark
[#]*These authors jointly initiated and supervised this work*
Supplemental data for this article can be accessed online at https://doi.org/10.1080/2162402X.2022.2158610

burden of random mutations and explain the necessity of more than 18 months of continuous thiopurine therapy. We recently showed that addition of low dose of 6TG to 6MP therapy (TEAM strategy) markedly increases DNA-TG levels,[16] and this strategy is approved for clinical testing (clinicaltrials.gov: NCT04307576).

Yale university low-mutational mouse melanoma (Yumm) cell line harboring *Braf*$^{V600E}$ mutation and *Pten* and *Cdkn2a* deletion[17] grow well in immunocompetent C57BL/6 mice, providing a valuable preclinical mouse model for cancer immunotherapy.[17,18] In this study, we provide data which indicate that treatment of Yumm1.1 cells with 6TG can markedly enhance the immune response toward our preclinical melanoma model and promote the response to ICI. We also establish that 6TG exposure improves tumor control on several mouse models. Collectively, our data can serve as a proof of concept for clinical use of the TEAM strategy in combination with ICI in otherwise treatment-resistant cancers with low TMB.

## Materials and methods

### *Mice*

Male C57BL/6 N (B6) mice were obtained from Taconic farms at the age of 8–10 weeks. The transgenic mouse model of melanoma used for the study were *Tyr::CreER*$^{T2/+}$;*Braf*$^{V600E/+}$; *Pten*$^{-/-}$ female and male on a C57BL/6 N background and bred inhouse.[19] Mice were housed at the ALAAC accredited animal facility at the Danish Cancer Society Research Center (Copenhagen, Denmark) and acclimated for a week before entering experiments. All animal care and mice experiments were performed in compliance with institutional guidelines and with protocols approved by the Danish animal experiments inspectorate (Dyreforsøgstilsynet, 2020–15-0201-00578).

## Mice monitoring-endpoints

Tumor volume, weight and health status were monitored regularly after cell injections, and mice were euthanized at endpoints. Tumor volumes were measured three times a week or daily by a digital caliper and were determined using the formula $(W \times L^2)/2$, where W > L and W = Width and L = Length. The endpoints for the experiment were defines as the time:

- tumors reached the maximum volume allowed by Danish legislation $[(W + L)/2 \geq 12]$
- critical ulcerations appeared on the tumor
- mice experienced weight loss exceeding 25% of the initial weight.

## Cell preparation

Yumm1.1 and Yumm1.7 cells were kindly provided by Dr Corine Bertolotto, INSERM, Biology and Pathologies of melanocytes, Center Méditerranéen de Médecine Moléculaire, Nice, France. For the *in vitro* characterization of Yumm1.1 cells, 5–10x10$^3$/400 µl of cells were seeded in 24 well plates. One day after seeding, cells were treated with different doses of 6TG (0.001–1 µg/ml). 6TG was obtained by Sigma-Aldrich and was reconstituted in 1 M NaOH to a stock concentration of 50 mg/ml. Control cells were treated with 0.02 M NaOH. On day 5 and/or 7, cells were processed for different assays. For the in vivo experiments involving Yumm1.1 cells, 1.5–2.5x10$^6$/10 ml cells were seeded in T75 flasks. One day after seeding, flasks were treated with 0.02 M NaOH (CTRL-Yumm1.1 cells) or 0.01–0.02 µg/ml 6TG (6TG-YummTG1.1 cells). When flasks were confluent (around day 4), cells were split 1:2 and retreated with NaOH or 6TG. On day 7, cells were collected in PBS and counted with a TC20 automated cell counter (Bio-Rad) and processed accordingly for injection in mice. For the *in vivo* experiment involving Yumm1.7 cells, 2.5x10$^5$/10 ml cells were seeded in T75 flasks. One day after seeding, flasks were treated with 0.02 M NaOH (CTRL-Yumm1.7 cells) or 0.02 µg/ml 6TG (6TG-YummTG1.7 cells). On day 5, cells were collected in PBS and counted with a TC20 automated cell counter (Bio-Rad) and processed accordingly for injection in mice.

## Cell proliferation and propidium iodide staining (PI)

For the *in vitro* characterization, a Celigo image cytometer (Nexcelom Bioscience) was used to take images of Yumm1.1 cells at day 5 and 7 post 6TG treatment. Cell counting was also achieved via the Celigo image cytometer and was expressed as total number of cells per well. For the *in vivo* experiments, a TC20 automated cell counter (Bio-Rad) was used to count the Yumm1.1 or Yumm1.7 to be seeded in T75 flasks (day 0). On day 7 and 5 respectively, cells were counted again and expressed as total number of cells.

The distribution of cells in the distinct phases of cell cycle (sub-G1, G1/S, G2/M) was analyzed by PI-staining in logarithmic (sub-G1) and linear (G1/S, G2/M) scale. Stained samples were acquired on BD FACSVerse (BD Biosciences) within 4 hours and were analyzed with Flowjo v.10.6.1.

## Mitochondrial membrane depolarization

Cells were seeded and treated with 6TG for 7 days as previously described. 30 min before the endpoint, cells were incubated at 37°C with MitoTracker Green FM and MitoTracker Red CMXRos (Invitrogen) according to manufacturer's instructions. As positive control we used the uncoupler CCCP (10 µM, 1 h). Cells were collected in PBS and were acquired on a Cytek Aurora (Cytek Biosciences Inc) and analyzed with Flowjo v.6.10.1. The polarization status of mitochondria was defined as the MFI ratios of MitoTracker Red/MitoTracker Green.

## DNA-TG levels MS

DNA was extracted from CTRL-Yumm1.1 and 6TG-YummTG1.1 and CTRL-Yumm1.7 and 6TG-YummTG1.7 cells using Omega E.Z.N.A. tissue DNA kit. DNA was also extracted from endpoint blood, bone marrow, spleen, and tumors. Levels of integrated DNA-TG were quantified by using Mass Spectrometry as previously described.[20,21] DNA-

TG levels were normalized to DNA quantity and expressed as fmol/µg of DNA.

## Syngeneic melanoma mouse models

For tumor inoculation, CTRL-Yumm1.1, 6TG-YummTG1.1, CTRL-Yumm1.7, and 6TG-YummTG1.7 cells were harvested at approximately 70–85% confluence on the day of injection. Cells were subsequently collected and resuspended in PBS/EDTA to the desired cell concentration of 300–600.000 cells/100 µl for CTRL-Yumm1.1 and 6TG-YummTG1.1 cells or 100.000 cells/100 µl for CTRL-Yumm1.7 and 6TG-YummTG1.7 cells. Mice were randomized based on weight and were injected with 100 µl of cell suspension subcutaneously into the right shaved rear flank using a 29 G insulin syringe. For the tumor growth curves, each data point corresponds to the average tumor volume of the mice in each experimental group.

## Transgenic mouse model of melanoma

For tumor induction, local administration of (Z)-4-Hydroxytamoxifen (4-OHT) (Sigma-Aldrich, MO, USA) in *Tyr::CreER*$^{T2/+}$;*Braf*$^{V600E/+}$;*Pten*$^{flox/flox}$ mice was induced by local application of 1.5 µl (7.8 mg/ml) of 4-OHT in EtOH onto the shaved dorsal skin of 3–4 week-old mice.[19] For the tumor growth curves, each data point corresponds to the average tumor volume of the mice in each experimental group for a given day after 4-OHT induction.

## Histological analysis

FFPE (Formalin Fixed Paraffin Embedded) tumor-sections of 4 µm were cut and stained according to standard staining procedures for Hematoxylin (Sigma-Aldrich), eosin (Sigma-Aldrich), and anti-Ki67 IHC (1:1000 Abcam). Digital images were acquired with a NanoZoomer-XR Digital slide scanner (Hamamatsu, JP) and NDP.view 2 software (v2.8.24) and quantified using QuPath (v0.3.0) to determine the percentage of Ki67-positive cells in the total area of the section. Data are expressed as mean ± SD. All the IHC of tumor sections were assessed by a pathologist (F.M.B.) blinded to the experimental conditions.

## TUNEL assay

To assess cell death, the TUNEL Assay Kit-BrdU-Red (Abcam, UK) was used following manufacturer's instructions. Tissue sections were deparaffinized, rehydrated, and treated with 20 µg/ml Proteinase K (ThermoFischer Scientific, MA, USA) for 5 min according to the kit's protocol. Nuclear staining was performed for 10 min at room temperature with 1 µg/ml Hoechst 33342. Images were taken using a Zeiss LSM800 confocal microscope. Each section was imaged in 4–5 different areas to acquire representative values.

## *In vivo* T cell depletion

The InVivoMab anti-mouse CD8a (YTS 169.4) purchased by BioXcell was used for *in vivo* depletion of CD8 T cells. Mice to be depleted were injected intraperitoneally (i.p.) with 200 µg of the antibody 1 day prior to subcutaneous (s.c.) cell injection and with 100 µg of antibody 1 and 4 days after and thereafter every 4–5 days till the completion of the experiment. The FTY720 drug purchased by Sigma-Aldrich was used for depletion of circulating CD4 and CD8 T cells. FTY720 was dissolved in the drinking water of mice to a concentration of 2.5 µg/ml and administered to them 2 days prior to s.c. cell injection and throughout the duration of the experiment. The efficiency of the cell depletion was confirmed by flow cytometric analysis of blood and/or splenocytes.

## Flow cytometry and antibodies

Single-cell suspensions from tumors/blood were stained for 30 mins (4°C in the dark) for relevant cell-surface markers in FACS staining buffer (PBS with 7% FBS). Next, the cells were washed, resuspended in PBS and stored at 4°C until flow cytometric analysis the same day. Samples were acquired on Cytek Aurora equipped with 4 lasers (Cytek Biosciences Inc) and analyzed with Flowjo v.10.6.1.

The following fluorochrome-conjugated Abs, purchased from Biolegend as anti-mouse antibodies, were used for flow cytometry surface staining: PE/Cy7-CD45 (30-F11), PerCP-cy5.5-CD3 (17A2), BV650-CD11b (M1/70), APC-CD8 (53–6.7), FITC-CD4 (GK1.5), BV605-CD19 (1D3), PE/Cy5-NK1.1 (PK136), BV421-CD25 (PC61), PE-PD1 (RMP1-30), BV785-PD-L1 (10 F.9G2), APC/Cy7-Ly6C (HK1.4), BV711-Ly6G (1A8). Live/dead cells were discriminated based on the Zombie Aqua Fixable Viability kit (BioLegend). To prevent unspecific binding, un-labeled anti-CD16/32 antibody was included.

## Anti-PD1/isotype control

One day after cell injections or when tumors reached measurable size (ca. 30 mm^3), mice were treated with 10 mg/kg of anti-PD1 (InVivoMab anti-mouse PD-1 (CD279), BioXcell) by intraperitoneal injection. Control animals were treated with 10 mg/kg of IgG2a isotype (InVivoMab rat IgG2a isotype control, BioXcell). Threafter, mice received injections twice weekly for approximately 4–5 weeks.

## Whole genome sequencing analysis

DNA extraction from CTRL-Yumm1.1 and 6TG-YummTG1.1 tumors as well as control YUMM1.1 cell line was performed using Qiagen's DNeasy Blood & Tissue Kit. Whole Genome Sequencing (WGS) was performed using the Illumina Novaseq 6000 platform. A bioinformatics pipeline for data analysis was developed on Computerome, the Danish National Computer for Life Sciences. WGS raw fastq files from tumor samples were aligned to the C57BL/6 J GRCm38 (mm10) mouse reference genome using the Burrows-Wheeler Alignment tool v.0.7.17.[22] Picard-tools v.2.26.106 and GATK v.4.2.5.0[23] were used for

BAM preprocessing. Somatic single-nucleotide variants and indels were identified using GATK's Mutect2.[24] Mutect2 was applied using the turmor-normal mode, using sample CTRL-Yumm1.1 cells BAM file as normal. Identified somatic variants were annotated with Annovar v.2019oct24,[25] using the mouse (mm10) reference genes from UCSC as reference. Finally, the R package Maftools[26] was used to calculate the tumor mutational burden (TMB), and to further analyze somatic variants in each tumor sample.

## RNA sequence analysis

For RNAseq analyses, RNA from tissues (disrupted with Qiagen Tissuelyser II) were isolated using the RNeasy Plus Mini Kit (Qiagen, DE), following the instructions of the manufacturer. When RNA from tissues could not be isolated immediately, tumor pieces were preserved in RNA*later*™ Stabilization Solution (ThermoFisher Scientific, MA, USA), according to the instructions. RNA sequencing was performed on bulk tumor extracts from CTRL-Yumm1.1 and 6TG-YummTG1.1 tumors with Illumina NextSeq, processed with the STAR aligner v2.7.9a.[27] and then used the R package DESeq2 v.1.32.0[28] for gene expression analysis. Functional analysis was performed with GSEA v4.2.3[29] and the gene set collections in the mouse Molecular Signature database (MSigDB) v2022.1.Mm, which includes 15,918 gene sets divided into 6 major collections, and several sub-collections. Gene set enrichments were tested running GSEA configured with the parameter permutation type set to gene set.

## Statistical evaluation

GraphPad Prism Software (version 9) was used for plotting graphs and performing statistical analysis. For comparison of more than two-groups, Tukey's multiple comparisons test was performed. Pairwise comparisons were carried out using a non-parametric Mann–Whitney U-test. For comparison of tumor growth kinetics, two-way-ANOVA with Bonferroni's multiple comparison test was performed. Data are presented as means ± SD and significance was designated as follows: $^{*}p \leq .05$; $^{**}p \leq .01$; $^{***}p \leq .001$; $^{****}p \leq .0001$; ns, not significant.

## Results

### *In vitro* characterization of the effects of 6TG treatment on Yumm1.1 cells

Amongst the characterized Yumm cell lines, the Yumm1.1 line has been shown to be poorly immunogenic with low response to immunotherapy[17,18] making it suitable for testing new strategies to improve clinical success with ICI therapy.

First, we sought to establish the optimal dose and duration of treating Yumm1.1 cells with thiopurine 6TG *in vitro*. To this purpose, we tested doses in the range between 0.001–1 µg/ml 6TG and assessed the effects on proliferation, cell cycle, cell death, metabolic activity, and DNA-TG integration on days 5 and/or 7 post treatment initiation (Figure 1a).

Cell viability, measured via Hoechst staining and Celigo image cytometer, indicated that the higher doses had an obvious cytotoxic effect on the cells (Figure 1b). Furthermore, cell cycle status, measured via Propidium Iodide (PI)-staining and flow cytometry, revealed a tendency for a dose-dependent G2-phase arrest and subG1 increase (Figure 1c-e). To have indication on the effects of 6TG treatment on cellular metabolic activity we used mitochondrial dyes that track mitochondrial mass (MitoTracker Green) and mitochondrial membrane potential (MitoTracker Red) (Figure 1f, g). The ratio of the mean fluorescence intensity (MFI) of the two dyes, detected by flow cytometry, is indicative of mitochondrial activity with decreases in the ratio being indicative of dysfunctional/depolarized mitochondria.[30] We observed that doses above 0.02 µg/ml 6TG significantly altered the metabolic profile of the treated cells whereas lower doses did not have a profound impact on metabolic activity (Figure 1f, g). We further measured the levels of thioguanine nucleotides (TGN) that were incorporated into the DNA (DNA-TG) of the treated cells via mass spectrometry (MS) analysis.[20] Higher 6TG treatment doses induced higher DNA-TG levels and the 0.01 µg/ml dose induced DNA-TG levels between 300 and 1200 fmol/µg DNA (Figure 1h), which is comparable with the DNA-TG levels obtained in ALL patients on thiopurine-based maintenance therapy.[15,31,32]

Additionally, we assessed the expression of apoptotic (Pro-Casp3) and immunogenic cell death (ICD) markers [Calreticulin (CRT) on cell surface and HMGB1 release in cell medium[33]] following treatment of Yumm1.1 cells with different concentrations of 6TG for 7 days *in vitro* (**Supplementary Figure 1**). Pro-Casp3 was measured by western blot and none of the 6TG concentration induced its cleavage, as opposed to treatment with high doses of the ICD-inducers Oxaliplatin and Doxorubicin[33] (**Supplementary Figure 1A**). Similarly, 6TG treatment did not induce increased levels of HMGB1 release in the cell medium, while cells treated with Doxorubicin had a more profound secretion of this protein, as detected by western blot (**Supplementary Figure 1B**). When we checked for CRT expression via flow cytometry, we found that doses above 0.05 µg/ml 6TG significantly increased the expression of CRT on the surface of Yumm1.1 cells, while the lower doses induced only background expression levels (**Supplementary Figure 1C**).

### Pre-treatment of Yumm1.1 cells with low doses of 6TG results in improved tumor control *in vivo*

Based on the *in vitro* assessment of 6TG effect on Yumm1.1 cells, we established that the 6TG treatment dose range with minimal toxic effect, which could suffice for clinical grade DNA-TG integration (>200 fmol/µg DNA) in Yumm1.1 cells, were 6TG doses between 0.01 and 0.02 µg/ml. Thereafter, we set out to monitor the *in vivo* progression of tumors established by injecting control (CTRL-Yumm1.1 cells) or 6TG pre-treated (6TG-YummTG1.1) cells in mice.

To this end, we cultured Yumm1.1 cells in the absence or presence of 6TG for a week and injected them subcutaneously into the right flank of immunocompetent C57BL6/N mice

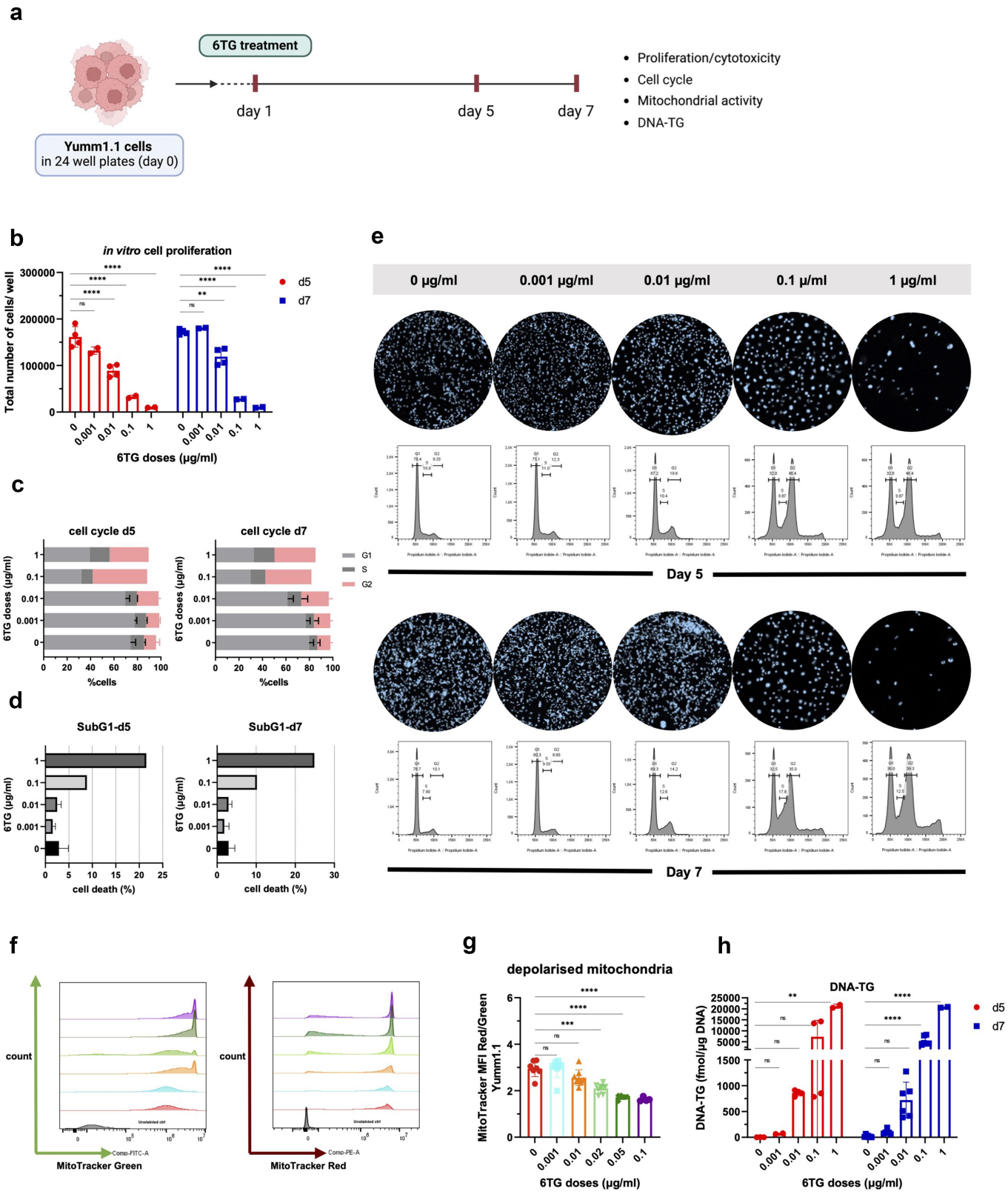


**Figure 1.** Effects of 6TG treatment on Yumm1.1 cells. A) Schematic representation of the experimental design (created with BioRender.com). Yumm1.1 cells were treated with different concentrations of 6TG. On days 5 and 7 cells were analyzed for B) cell proliferation via Hoechst staining and Celigo imaging (n = 2–4), C) cell cycle on days 5 and 7 via PI staining and flow cytometric analysis (n = 1–4), D) % of subG1 on days 5 and 7 via PI staining and flow cytometric analysis (n = 1–4). E) Representative images from Celigo imaging and cell cycle status on day 7, for the tested 6TG concentrations. F) On day 7, we assessed the degree of depolarized mitochondria in cells under 6TG treatment with different concentrations of 6TG as a ratio between MFI of Red/Green mitotracker (n = 4–8). G) Representative flow of Mitotracker Green (identifying mitochondrial mass) and Mitotracker Red (identifying mitochondrial potential) for the tested 6TG concentrations. H) Levels of DNA-TG were assessed by MS on extracted DNA from cells on days 5 and 7 (n = 2–6). Each dot represents one measurement. Data are pooled from several independent experiments and are presented as mean ± SD.

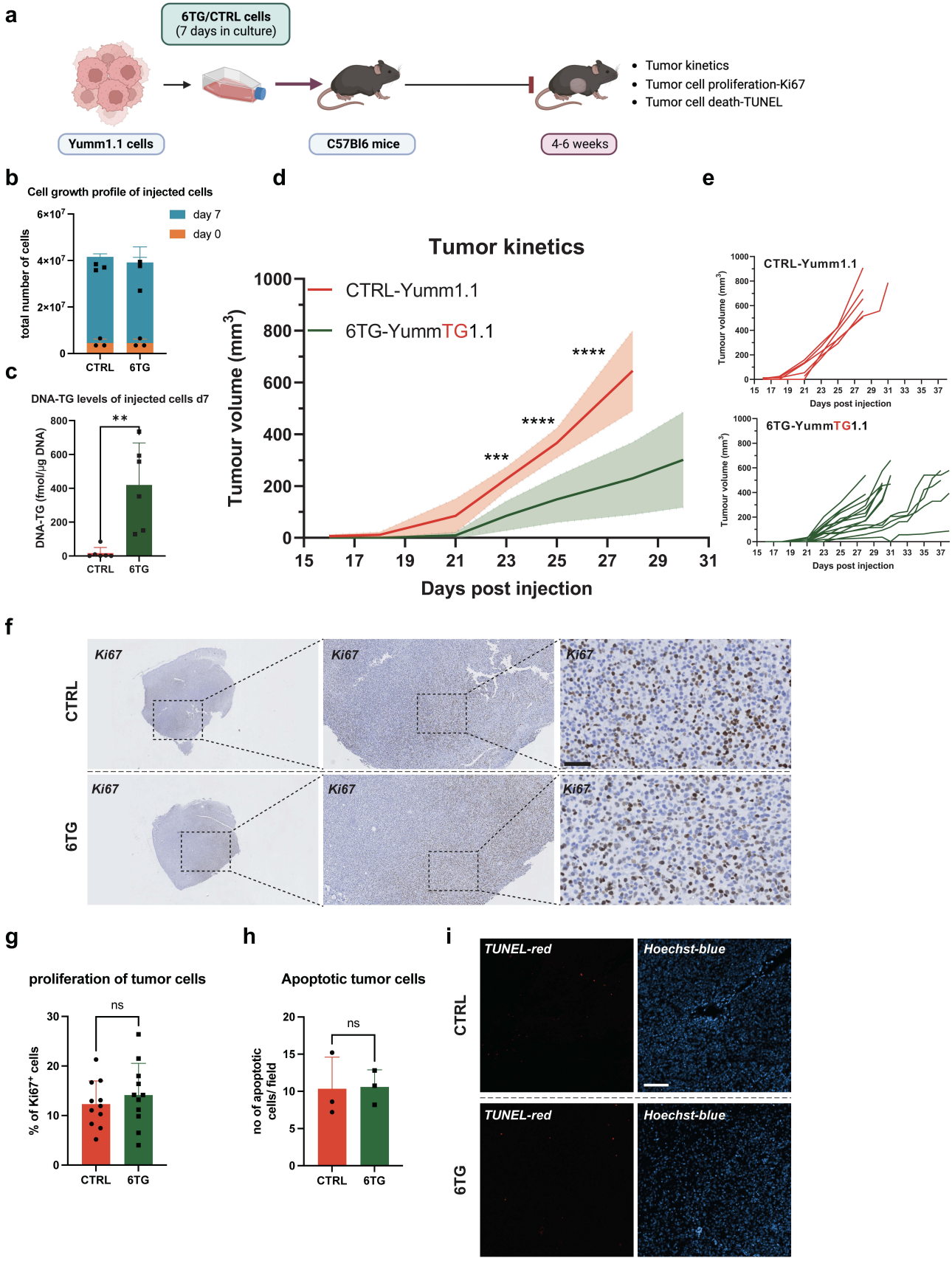


**Figure 2.** *In vivo* progression of CTRL-Yumm1.1 and 6TG-YummTG1.1 tumors. A) Schematic representation of the experimental design (created with BioRender.com). Yumm1.1 cells were treated (6TG-YummTG1.1) or not (CTRL-Yumm1.1) with 6TG and after 7 days, cell growth (B) and DNA-TG integration (C) were assessed (n = 3–6). Each dot represents one sample/experiment. Results are pooled from 6 independent experiments and are presented as mean ± SD. D) Tumor kinetics following injection of 250.000–300.000 CTRL-Yumm1.1 and 6TG-YummTG1.1 cells in mice (n = 6–15). Half of the mice receiving 6TG-YummTG1.1 cells, additionally received 2 µg/ml of 6TG in the drinking water. Each data point corresponds to the mean tumor volume ± SD, as determined for each experimental group. E) Tumor kinetics of individual mice in CTRL-Yumm1.1 (n = 6) and 6TG-YummTG1.1 groups (n = 15). F, G) The proliferation rate of tumor cells was assessed by Ki67$^{+}$ IHC staining of FFPE-tumor sections from

(Figure 2a). Analysis of the cells collected at day 7 (i.e., prior to the injection) confirmed that 6TG treatment induced clinical-grade DNA-TG integration without impacting the cellular proliferation of the injected cells (Figure 2b, c). Tumor growth was monitored over time and, at the endpoints, tumors were collected and stored appropriately for the different assays. The tumor kinetics revealed a treatment-response pattern in which 6TG-YummTG1.1 tumors appeared later and were smaller in comparison to CTRL-Yumm1.1 tumors (Figure 2d, e).

We performed Ki67 staining of tumor sections to assess whether 6TG pre-treatment of Yumm1.1 cells altered the cellular phenotype in a way that impacted their proliferation rate *in vivo*. We observed that 6TG-YummTG1.1 and CTRL-Yumm1.1 tumor cells had similar proliferation rates, thus pointing toward the direction of the tumor control being immune-mediated (Figure 2f, g). In addition, we assessed the tumor cell mortality rate using the TUNEL assay on tumor sections from CTRL-Yumm1.1 and 6TG-YummTG1.1 groups. The results showed a similar low apoptotic cell rate between the groups (Figure 2h, i), which was in agreement with the *in vitro* analysis data showing that our chosen 6TG pre-treatment doses had minimal toxic effects and induced background levels of apoptotic and ICD markers (Figure 1d and **Supplementary Figure 1**).

In an attempt to improve our model to better mimic the clinical situation, we evaluated the effect of administering 6TG via drinking water or oral gavage to the mice receiving untreated Yumm1.1 cells (**Supplementary Figure 2**). We assessed the maximum tolerated doses of 6TG and found that concentrations above 2 μg/ml in the drinking water and above 12.5 μg daily via oral gavage, caused significant weight loss (data not shown).

We observed that administration of the systemically tolerated 6TG doses, either via drinking water or oral gavage, significantly improved tumor control of mice receiving untreated CTRL-Yumm1.1 cells, though to a lesser extent than mice engrafted with 6TG pretreated cells (**Supplementary Figure 2A, B**). Furthermore, short-term exposure to 6TG through drinking water did not significantly increase DNA-TG in the established tumors or other tissues (**Supplementary Figure 3**). This most likely reflects the dilution of DNA-TG accumulated during the *in vitro* pre-treatment of the tumor cells with each division after injection as well as the insufficient exposure to 6TG through the drinking water (3–4 weeks). Therefore, as our main model, we kept on injecting mice with Yumm1.1 cells pre-treated with 6TG (6TG-YummTG1.1). Moreover, the additional administration of 6TG via drinking water to the mice receiving 6TG-YummTG1.1 cells had a positive, though not significant, impact on the inhibition of tumor growth (**Supplementary Figure 2A**). Therefore, in most of the subsequent *in vivo* experiments, 6TG was also administered in the drinking water of the 6TG-YummTG1.1 group. Specific details are provided in the figure legends.

## 6TG-induced tumor control correlates with increased TMB and upregulation of immune-related pathways

According to our hypothesis, the DNA-TG levels of the injected cells led to the accumulation of sufficient mutations that contributed to the observed improved 6TG-YummTG1.1 tumor control. To verify that 6TG-YummTG1.1 tumors had increased tumor mutation burden (TMB) compared to CTRL-Yumm1.1 tumors, we extracted DNA from tumors at endpoint and performed whole genome sequencing (WGS). The sequencing data analysis revealed that the mean TMB of CTRL-Yumm1.1 tumors was 4.06 mutations per megabase (mut/Mb), whereas the mean TMB of 6TG-YummTG1.1 tumors was 5.35 mut/Mb (i.e., a 31% increase of the TMB) (Figure 3a). When correlating the TMB with tumor volumes at day of sacrifice, we observed that within the 6TG-YummTG1.1 group, mice with higher TMB tend to have smaller tumor volumes (Figure 3b, 3c). These findings are compatible with previous clinical studies that link high TMB to greater levels of neoantigens and enhanced tumor control.[34]

Next, to gain further insights into the processes affected by 6TG exposure, we performed RNA sequencing of CTRL-Yumm1.1 and 6TG-YummTG1.1 tumors at endpoint. Gene set enrichment analysis (GSEA) revealed an enrichment of gene sets in the 6TG-YummTG1.1 tumors, which were involved in cytokine activity, chemokine activity, chemokine receptor binding, myeloid and leukocyte activation, inflammatory response, TNFα signaling, and IFNγ response (Figure 3d).

These results indicate that the tumor growth suppression induced by 6TG is associated with increased TMB and the activation of immune-related pathways.

## CTRL-Yumm1.1 and 6TG-YummTG1.1 tumors have distinct immune microenvironments

Next, we explored whether the tumor immune microenvironment differed between the two groups. To address this, tumors from CTRL-Yumm1.1 and 6TG-YummTG1.1 groups were collected at endpoint and processed for flow cytometric analysis (**Supplementary Figure 4, 5**). We observed a significant increase in the frequency of CD45 cells, lymphoid cells and myeloid cells within the 6TG-YummTG1.1 tumors (Figure 4a-d, 4g). When we focused on the lymphoid subset, we further detected increases in the frequency of CD8 T, CD4 T and NK cells (Figure 4d). The expression of the activation/exhaustion marker PD1 tended to be elevated on CD8 T cells ($p = .054$) and CD4 T cells ($p = .04$) (Figure 4e), and the population of $CD25^+$CD4 T cells was enriched (Figure 4f). 6TG-YummTG1.1 tumors also had a higher frequency of $PDL1^+$ myeloid and myeloid derived suppressor cells (MDSCs, $Ly6C^+$ myeloid cells) (Figure 4g).

CTRL-Yumm1.1 and 6TG-YummTG1.1 mice (n = 11). F) Representative Ki67 IHC staining for each group. Scale bar = 50 μm. G) Results are pooled from two independent experiments. Each dot represents one mouse and data are presented as mean ± SD of $Ki67^+$ cells on nuclei count for each mouse. H, I) TUNEL assay was used to determine cell death in FFPE-tumor sections from CTRL-Yumm1.1 and 6TG-YummTG1 mice (n = 3). H) Each dot represents one mouse and data are presented as mean ± SD of apoptotic cells per counting field for each section. I) Representative images of TUNEL staining. Apoptotic cells are shown as red (BrdU) and nuclei are shown as blue (Hoechst). Images are representative of each group. Scale bar = 200 μm.

a

| | CTRL-Yumm1.1 | 6TG-YummTG1.1 |
|---|---|---|
| mean TMB | 4.06 mut/Mb | 5.35 mut/Mb |
| % increase | - | 31 % |

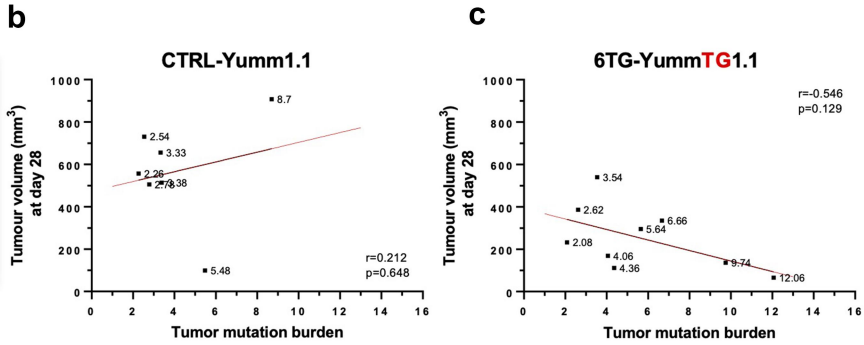


d

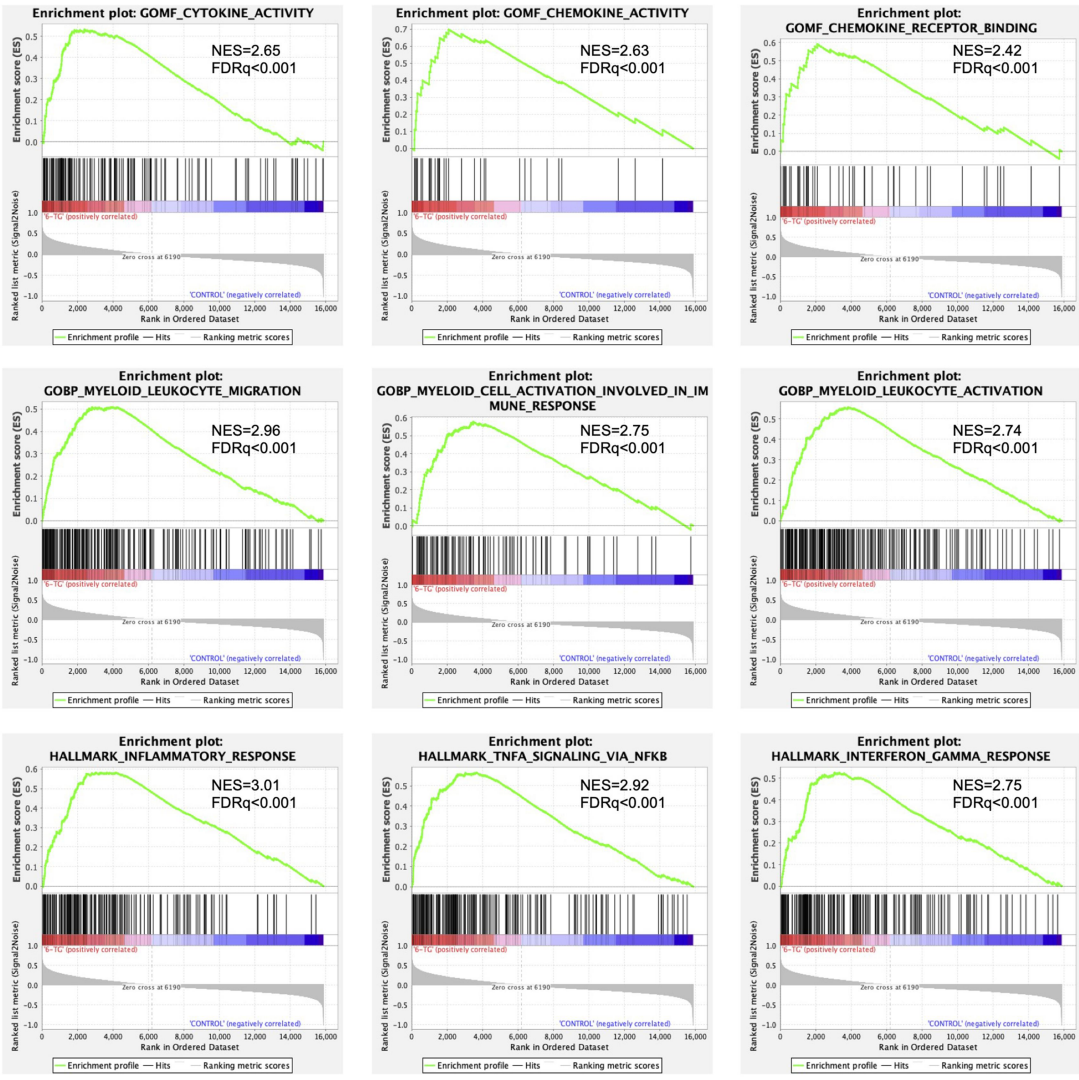


**Figure 3.** TMB and GSEA of CTRL-Yumm1.1 and 6TG-YummTG1.1 tumors. A) Table presenting the mean TMB assessed at the endpoint on CTRL-Yumm1.1 and 6TG-YummTG1.1 tumor-DNA (n = 7–10). B) Correlation between TMB and tumor volumes at day 28 for CTRL-Yumm1.1 group (n = 7). C) Correlation between TMB and tumor volumes at day 28 for 6TG-YummTG1.1 (n = 10). D) GSEA enrichment plots from different enriched gene sets [GO_Molecular Factor (GOMF), GO_Biological Process (GOBP), Hallmark] in the CTRL-Yumm1.1 and 6TG-YummTG1.1 tumor samples (n = 7–10). NES, normalized enrichment score; FDR, false discovery rate.

These results suggested that the increase in T cell and NK cell infiltration in the 6TG-YummTG1.1 tumors contributed to the observed improved tumor growth control. Nevertheless, tumor progression was not completely suppressed, possibly due to elevated levels of MDSCs and $CD25^{+}CD4$ T cells, which are known to promote tolerance.[35]

## 6TG exposure impacts tumor growth in other mouse models of melanoma

To ensure that the tumor control observed in our model upon 6TG treatment was reproducible in other mouse models of melanoma, we evaluated the tumor growth kinetics upon 6TG exposure in a syngeneic mouse model engrafted with

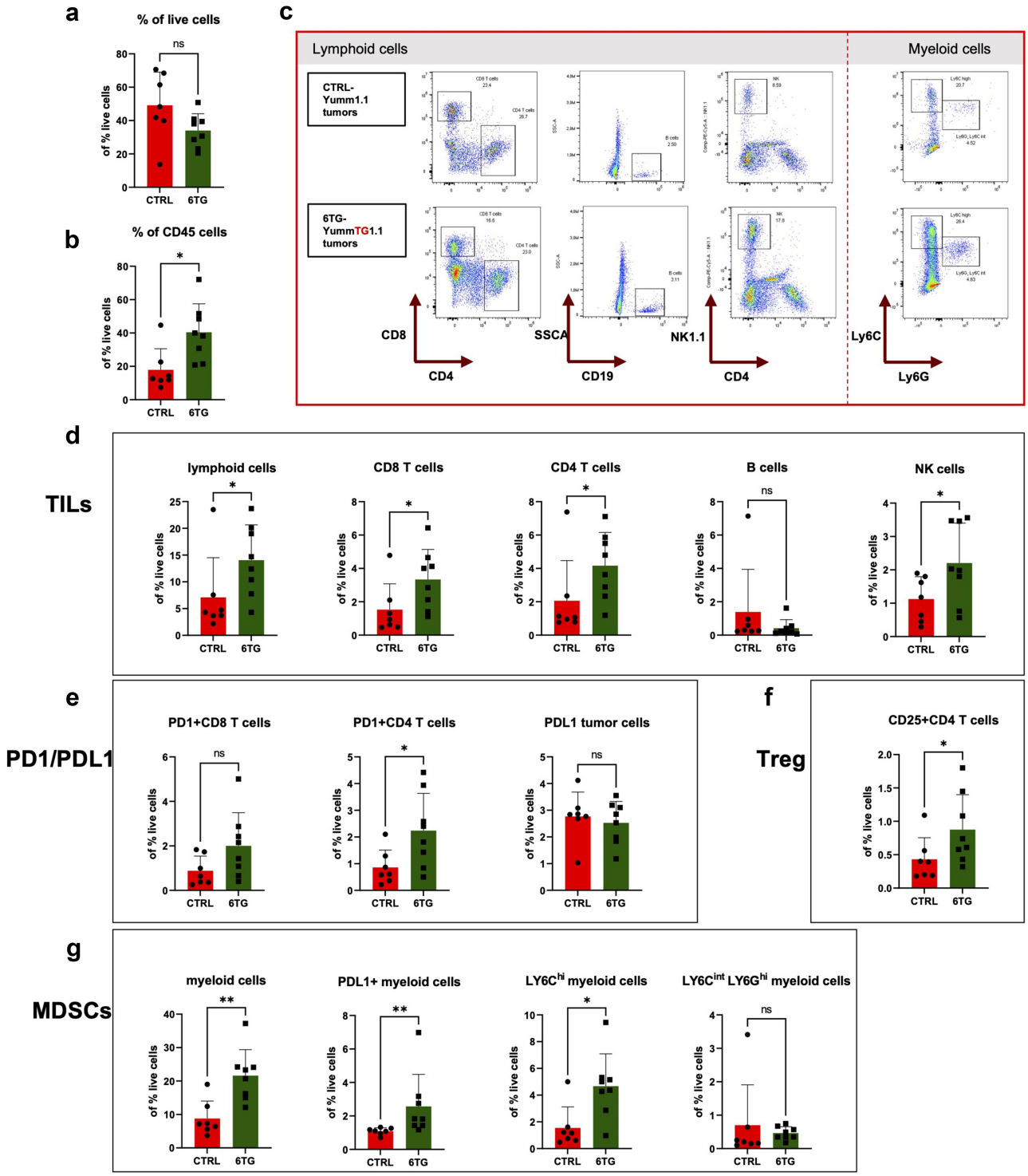


**Figure 4.** Analysis of tumor microenvironment in CTRL-Yumm1.1 and 6TG-YummTG1.1 groups. At endpoints, tumors from CTRL-Yumm1.1 and 6TG-YummTG1.1 groups were collected and processed for flow cytometric analysis. Gating strategy is shown in Supplementary Figures 4 and 5. A) % of live cells B) % of CD45 positive cells out of the live cell population. C) Representative flow plots on the gating strategy of lymphoid and myeloid cells in CTRL-Yumm1.1 and 6TG-YummTG1.1 groups. D) % of lymphoid cells (defined as $CD45^{hi}CD11b^{low}$) and the % of TILs: CD8 T, CD4 T, B, and NK cells out of the live cell population. E) % of PD1+ CD8 T, PD1+ CD4 T and PDL1 tumor cells out of the live cell population. F) % $CD25^{+}$CD4 T cells out of the live cell population. G) % of myeloid cells (defined as $CD45^{hi}CD11b^{hi}$), % of PDL1+ myeloid cells and the % of MDSC: $Ly6C^{hi}$ myeloid and $Ly6C^{int}Ly6G^{hi}$ myeloid cells out of the live cell population. Results are pooled from two independent experiments (n = 7–8). Each dot represents one mouse and corresponds to the mean ± SD.

Yumm1.7 melanoma cells[17] and a transgenic mouse model of inducible melanoma[19] (Figure 5).

For the syngeneic mouse model, we pre-treated Yumm1.7 cells in the absence (CTRL-Yumm1.7) or presence of 6TG (6TG-YummTG1.7) for 5 days prior to subcutaneous injection into the right flank of immunocompetent C57BL6/N mice (Figure 5a). The optimal duration and concentration of Yumm1.7 pre-treatment with 6TG was established based on its effect on cell proliferation and DNA-TG integration (**Supplementary Figure 6**). Following cell injections, tumor

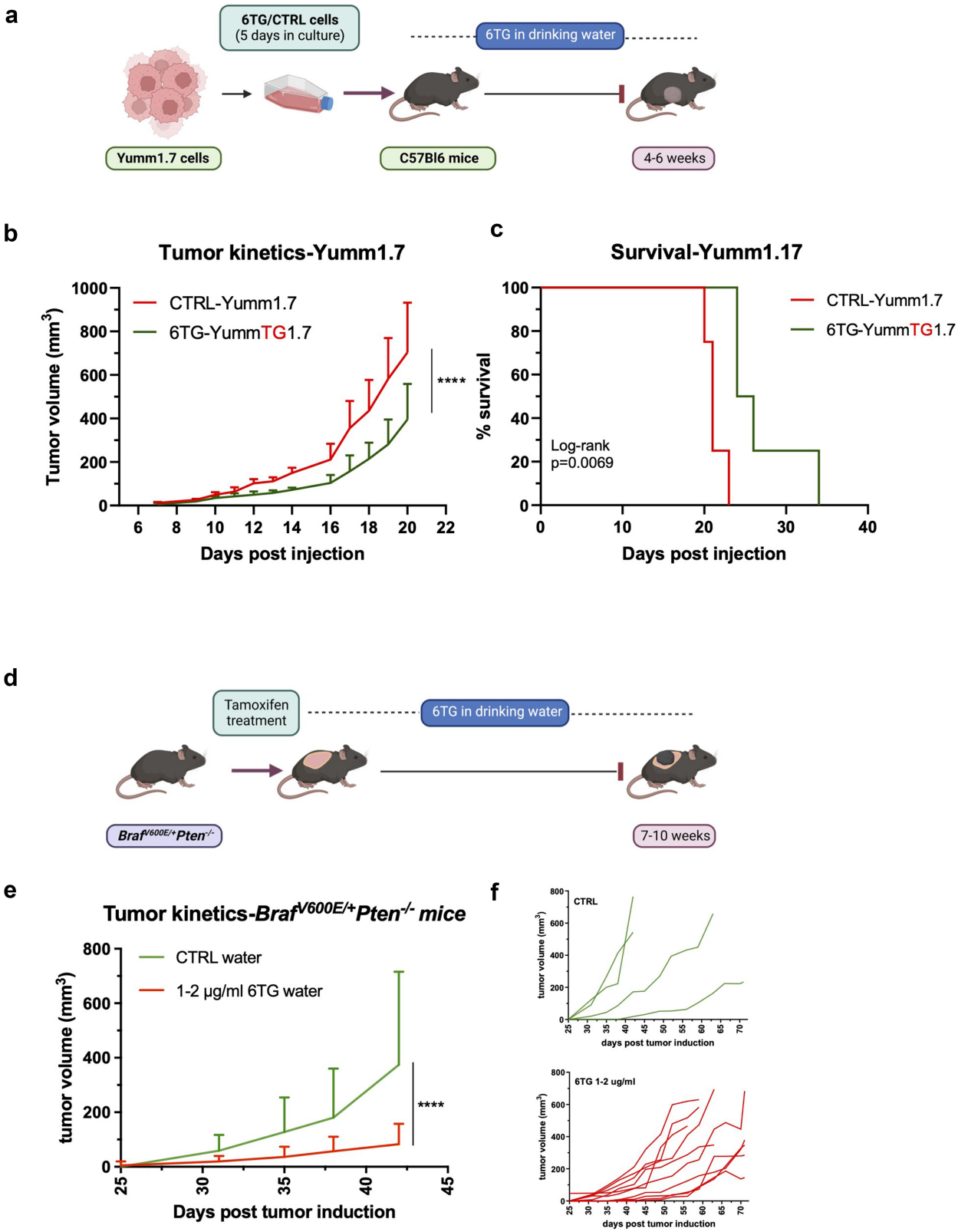


**Figure 5.** Reproducibility of 6TG effect in mouse models of melanoma. A) Schematic representation of the experimental design for the syngeneic mouse model using Yumm1.7 cells (created with BioRender.com). Yumm1.7 cells were treated (6TG-YummTG1.7) or not (CTRL-Yumm1.1) with 6TG and after 5 days, 100.000 cells were injected in mice. Mice receiving 6TG-YummTG1.1 cells, additionally received 2 µg/ml of 6TG in the drinking water. B) Tumor kinetics was assessed over time (n = 4). Each data point corresponds to the mean tumor volume ± SD, as determined for each experimental group. C) Kaplan-Meier survival curve for 6TG-YummTG1.7and 6TG-YummTG1.7 groups. As endpoint was defined the date the mice reached tumor max size (n = 4). D) Schematic representation of the experimental design for the transgenic mouse model of melanoma (created with BioRender.com). *Braf*$^{V600E/+}$*Pten*$^{-/-}$ mice were treated with tamoxifen (4-OHT) and tumor formation was followed over time. Mice were administered 1–2 µg/ml of 6TG in the drinking water. A group of control mice receiving CTRL water was included. E) Tumor kinetics was assessed over time (n = 4–10). Each data point corresponds to the mean tumor volume ± SD, as determined for each experimental group. F) Tumor kinetics of individual mice in CTRL-water (n = 4) and 6TG-water (n = 10) groups.

growth was monitored over time and revealed that 6TG-YummTG1.7 tumors were better controlled and the mice had a survival advantage compared to CTRL-Yumm1.7 (Figure 5b, c).

For the transgenic mouse model, we induced tumor formation by local administration of tamoxifen onto the shaved dorsal skin of *Tyr::CreER*$^{T2/+}$;*Braf*$^{V600E/+}$;*Pten*$^{flox/flox}$ mice.[19] Following tamoxifen treatment, mice received control (CTRL) or 6TG (1–2 µg/ml 6TG) via drinking water and their tumor growth was monitored over time (Figure 5d). Tumor kinetics revealed that 6TG administration via drinking water had a beneficial effect on tumor control Figure 5e, f).

Collectively, these data highlight that 6TG exposure consistently improves tumor control across different models.

## T cells are essential for keeping 6TG-YummTG1.1 tumors in check

To assess the direct role of T cells in the observed tumor growth control in the 6TG-YummTG1.1 group, we performed *in vivo* depletion of the circulating CD4 and CD8 T cells via administration of FTY720,[36,37] which inhibits lymphocyte egress from thymus and lymph nodes, in the drinking water and anti-CD8 antibody (αCD8) intraperitoneally (i.p.) (Figure 6a). Successful T cell depletion was evaluated by flow cytometric analysis in blood throughout the experiment (data not shown) and at endpoint (Figure 6b). The absence of both T cell subsets significantly accelerated tumor growth of the 6TG-YummTG1.1 tumors, while this was not the case for the CTRL Yumm1.1 group (Figure 6c). These results implied that the 6TG-YummTG1.1 group had superior tumor control due to adaptive immune responses involving T cells.

Next, we selectively depleted CD8 T cells in both CTRL-Yumm1.1 and 6TG-YummTG1.1 tumor-bearing mice (Figure 6d) and found that CD8 T cells depletion alone in the 6TG-YummTG1.1 group had the same effect on loss of tumor growth control as the combined depletion of CD4 and CD8 T cells, whereas the CTRL Yumm1.1 group was unaffected (Figure 6e).

## Anti-PD1 treatment improves immune control of 6TG-YummTG1.1 tumors

After establishing that 6TG-YummTG1.1 tumor control was immune mediated, we assessed whether ICI treatment with anti-PD1 antibody would further improve tumor control in this group. To this end, we established CTRL-Yumm1.1 and 6TG-YummTG1.1 tumors by injecting 300.000 cells in the right flank of immunocompetent C57BL6/N mice (Figure 7a). Mice were monitored daily and, upon appearance of palpable tumors, mice belonging to the 6TG-YummTG1.1 group were randomly assigned to receive isotype control or anti-PD1 i.p. injections twice weekly until the completion of the experiment. In line with our previous results, 6TG-YummTG1.1 tumors were better controlled than CTRL-Yumm1.1 tumors. Anti-PD1 treatment was able to further improve tumor control of 6TG-YummTG1.1 tumors, and while tumor volumes remained relatively similar (approximately 200 $mm^3$) for almost 4 weeks for both anti-PD1 and isotype control group, the anti-PD1 treated 6TG-YummTG1.1 tumors were better controlled in the later phases (Figure 7b).

To investigate if we could further improve the outcome of anti-PD1 treatment, we increased the number of injected cells from 300.000 cells to 600.000 cells and tested the effect of anti-PD1 treatment. We additionally assessed whether the timing of anti-PD1 treatment initiation could give an advantage to the immune system and have a stronger effect on tumor control. To this purpose, mice inoculated with either 600.000 CTRL-Yumm1.1 or 6TG-YummTG1.1 cells, were randomly assigned to receive isotype control or anti-PD1, starting already one day after cell injection. Thereafter and until the completion of the experiment, mice received isotype control or anti-PD1 injections twice weekly. We observed that the growth of CTRL-Yumm1.1 tumors was not impacted by anti-PD1 therapy, as previously reported,[18,38] while growth of 6TG-YummTG1.1 tumors was significantly delayed (Figure 7c-d). Anti-PD1 treatment was not able to cause the 6TG-YummTG1.1 tumors to regress, presumably due to the presence of immune cells with immunosuppressive properties as displayed in Figure 4f, g. In addition, we assessed the effect of anti-PD1 treatment when mice were exposed to 6TG exclusively via oral gavage daily and we did not find any significant difference (**Supplementary Figure 7**).

Overall, these results support that 6TG treatment promotes the antitumor response of PD1 blockade, and anti-PD1 therapy can partially overcome potential immunosuppressive mechanisms in the 6TG-treated tumors.

## Discussion

In this study, we performed a proof-of-concept analysis investigating whether a chemotherapy agent can increase the mutational burden and ultimately contribute to enhanced efficiency of ICI therapy. Our results offer an innovative titratable treatment strategy for patients with cancers that are otherwise responsive to ICI when TMB is high, but who currently cannot be offered ICI due to a low TMB. This strategy is now being tested in clinical phase 1/phase 2 trial (TEMPLE = Thiopurine Enhanced Mutations for PD-1/Ligand-1 Efficacy; NCT05276284).

In addition to a direct anti-cancer effect, chemotherapy also impacts anti-cancer immune responses, and there is now emerging evidence from phase III clinical trials to support combinations of immunotherapy with standard-of-care chemotherapy for several malignant diseases.[39] Thiopurines have been part of the success story of chemotherapy since 1953 and are widely used in the clinic as a low-toxic treatment for hematological malignancies and immunological disorders. In particular, 6MP is part of the 1–2 years maintenance therapy of ALL. The mechanism of action involves the integration of thiopurine metabolites (TGN) into the DNA (DNA-TG) in competition with natural guanine. DNA-TG can sit silently in the DNA without altering the nucleotide sequence but can occasionally become S-methylated and mismatch with thymidine. This mismatching will subsequently activate the MMR system which, after futile attempts to restore the correct nucleotide sequence, could lead to cell death. However, not all mismatches are efficiently recognized by the MMR mechanism,[40,41] and this

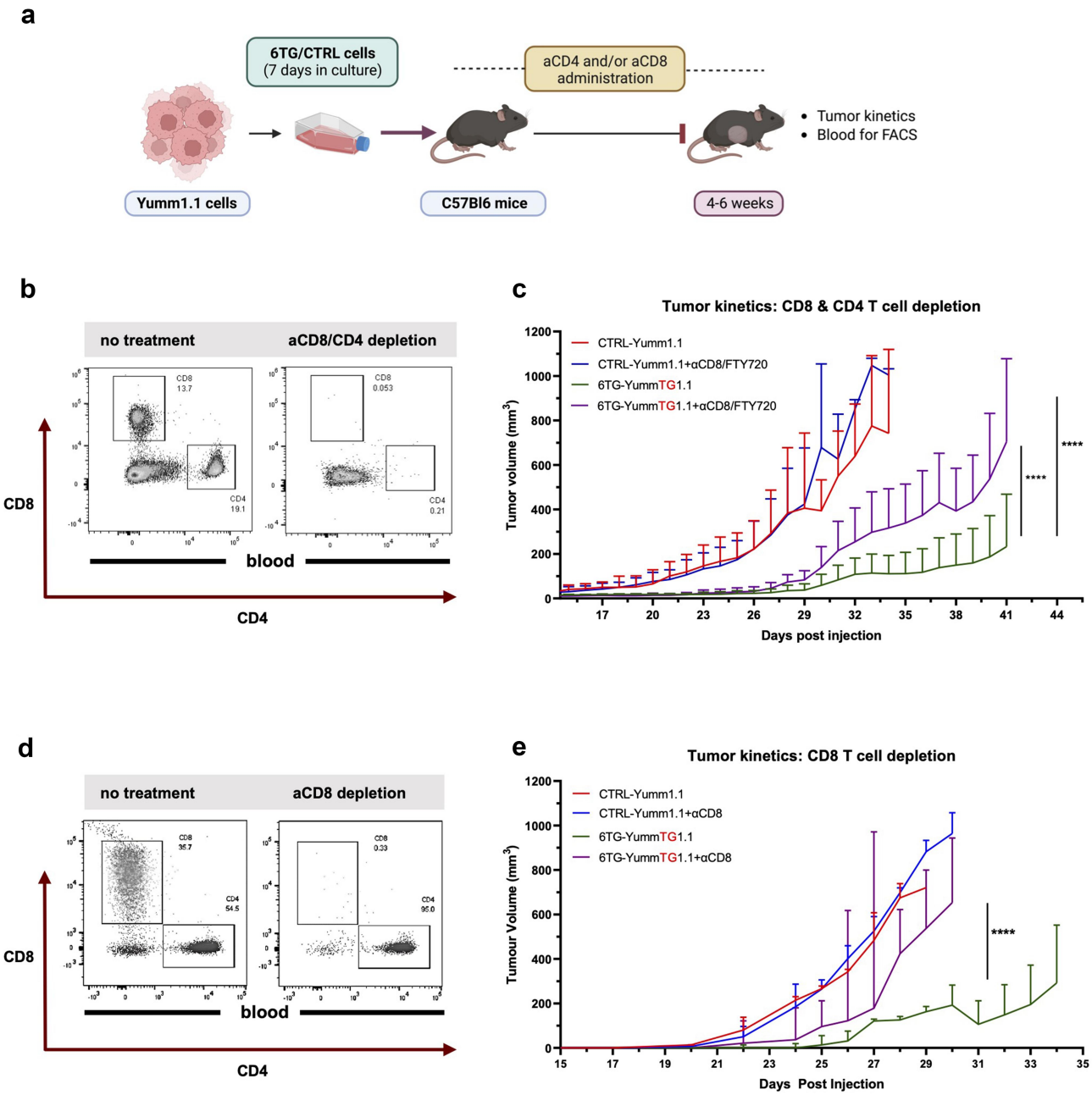


**Figure 6.** T cells depletion in CTRL-Yumm1.1 and 6TG-YummTG1.1 tumors. A) Schematic representation of the experimental design (created with BioRender.com). Yumm1.1 cells were treated (6TG-YummTG1.1) or not (CTRL-Yumm1.1) with 6TG and after 7 days 250.000–300.000 cells were injected in mice. B) Representative flow plot illustrating efficient depletion of circulating CD8 T and CD4 T cells in CTRL-Yumm1.1 and 6TG-YummTG1.1 groups. C) Tumor kinetics in CTRL-Yumm1.1 and 6TG-YummTG1.1 groups in the presence or absence of CD8 T and CD4 T cells (n = 8–9). D) Representative flow plot illustrating efficient depletion of circulating CD8 T cells in CTRL-Yumm1.1 and 6TG-YummTG1.1 groups. E) Tumor kinetics in CTRL-Yumm1.1 and 6TG-YummTG1.1 groups in the presence or absence of CD8 T cells (n = 3–4). Each data point corresponds to the mean tumor volume ± SD, as determined for each experimental group.

will eventually result in an increase in the number of accumulated mutations. The Nordic/Baltic NOPHO ALL2008 maintenance therapy study in 918 children established the association between relapse-free survival and a higher concentration of DNA-TG and demonstrated that the relapse risk was reduced by 28% for every 100 fmol/µg increase in DNA-TG levels.[14] The addition of low doses of thiopurine 6TG to the current maintenance therapy regime (6MP/MTX) was shown to significantly increase DNA-TG levels without increasing side-effects.[16] This strategy is called Thiopurine Enhanced ALL Maintenance (TEAM) and was tested in a pilot study including 34 patients.[15] Our hypothesis is that increased DNA-TG levels in the tumor cells likely result in an increasing number of mutations, which can be translated into neoantigens that can stimulate antitumor immune responses. Naturally, our next goal is to use the TEAM strategy to improve ICI outcomes in patients, but before proceeding with the clinical trial, we first wanted to confirm the rationale behind the study design in a preclinical mouse model.

In this study, we took advantage of a syngeneic mouse model of melanoma where we established tumors with a low mutational burden by injecting Yumm1.1 cells in

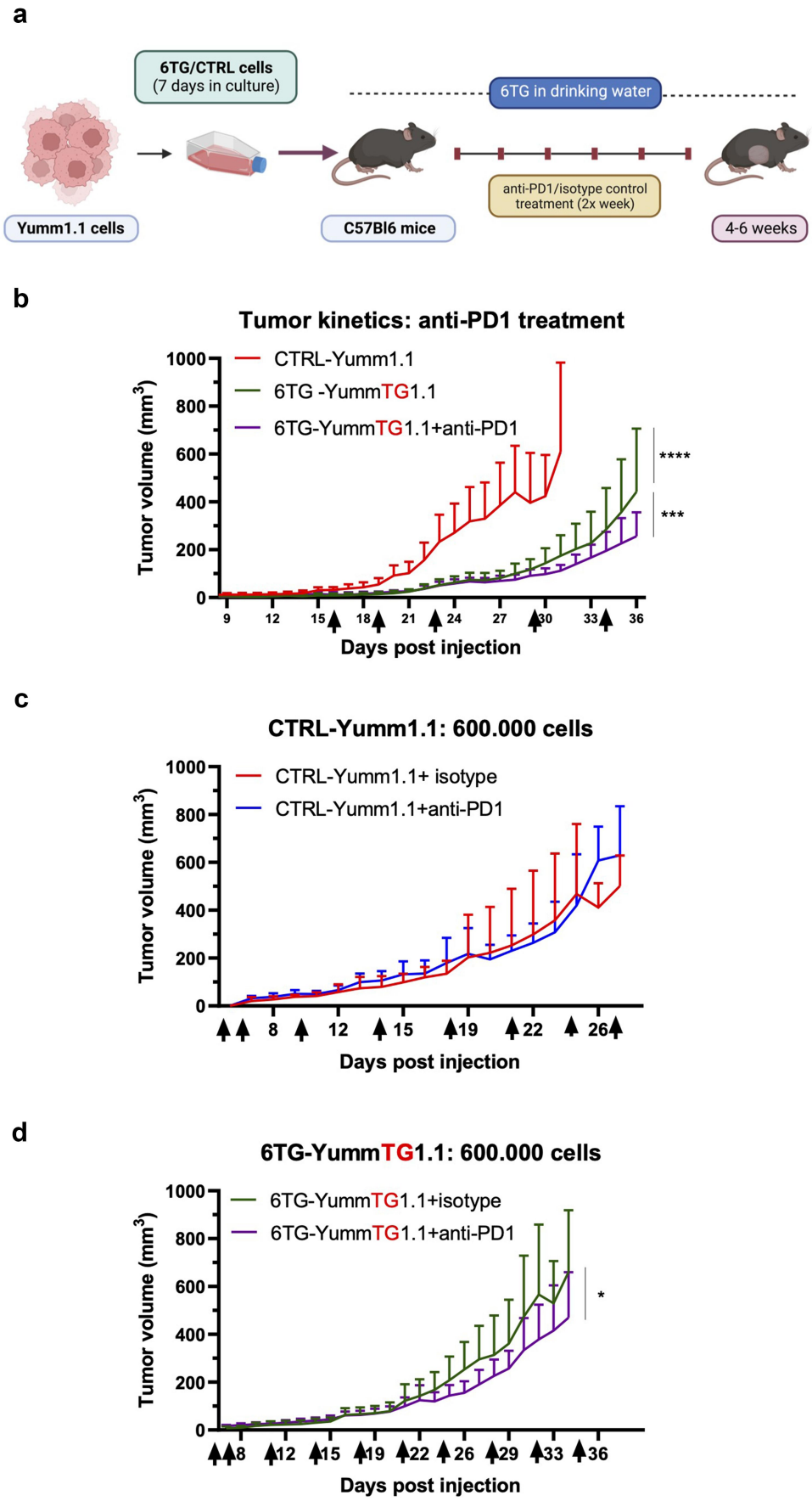


**Figure 7.** Anti-PD1 treatment of CTRL-Yumm1.1 and 6TG-YummTG1.1 tumors. A) Schematic representation of the experimental design (created with BioRender.com). Yumm1.1 cells were treated (6TG-YummTG1.1) or not (CTRL-Yumm1.1) with 6TG and after 7 days 300.000–600.000 cells were injected in mice. Mice receiving 6TG-YummTG1.1 cells, additionally received 2 µg/ml of 6TG in the drinking water throughout the experiment. B) Tumor kinetics in mice receiving 300.000 CTRL-Yumm1.1 or 6TG-YummTG1.1 cells. When tumors were measurable, mice in the 6TG-YummTG1.1 group were assigned to received anti-PD1/isotype injections approximately twice

immunocompetent mice. Yumm1.1 cells have been formerly characterized as poorly immunogenic, inducing low numbers of immune cell infiltration in the tumor and non-responsive to ICI therapy.[17,38] We used thiopurine 6TG to pre-treat the Yumm1.1 cells before injection into mice with the aim of increasing the TMB of the tumor and, in this way, reshaping the tumor microenvironment into a more immunogenic composition.

While the increased TMB does not necessarily guarantee that the right neoantigens will be presented on MHC-I on tumor cells, it will increase that likelihood.[7,42,43] To reinforce our hypothesis that increased 6TG exposure could lead to improved activation of the adaptive immune system, we performed *in vivo* T cell depletions in CTRL-Yumm1.1 and 6TG-YummTG1.1 tumor-bearing mice. We found that 6TG-YummTG1.1 tumor control was reduced in the absence of T cells, whereas CTRL-Yumm1.1 tumors exhibited similar growth kinetics in the presence or absence of T cells. Of note, CD8 T cell depletion alone had a similar effect on 6TG-YummTG1.1 tumor control to combined CD4 and CD8 T cell depletion, which might imply that CD8 T cells were the most critical component of the antitumor immune response. We further demonstrated that 6TG-YummTG1.1 tumors had immunologically distinct immune microenvironments compared to CTRL-Yumm1.1 tumors and were characterized by a substantial increase in immunogenic infiltrates (CD4 T, CD8 T and NK cells), but also an increase in immune cells with immunosuppressive properties (Ly6C$^{hi}$ myeloid cells, CD25$^{+}$CD4 T cells). In line with these results, we also demonstrated that the 6TG-YummTG1.1 tumors were enriched for cytokine/chemokine activity, inflammatory response, TNFα signaling, and IFNγ response, as well as for myeloid and leukocyte activation and migration gene signatures. In combination with the T cell depletion studies, we were able to conclude that 6TG-YummTG1.1 tumors were controlled mainly through activated T cell responses. We anticipated that, while the T cell responses kept the tumors in check, the presence of immune suppressive cells obstructed complete tumor regression. It is worth noting that all flow cytometric analysis was performed on tumors at endpoint, a stage where cancer cells have entered the so-called "immune escape" phase and the immune system is failing to effectively control tumor growth.[44] It would be very informative to monitor the kinetics of immune cell infiltration in the tumor over time after cell injection of CTRL-Yumm1.1 and 6TG-YummTG1.1 cells.

To illustrate that the beneficial effects of 6TG exposure are not restricted to our model, we successfully validated our observations in additional melanoma mouse models, *e.g.* the syngeneic mouse model engrafted with 6TG-pretreated Yumm1.7 cells and the transgenic mouse model of inducible melanoma (*Tyr::CreER*$^{T2/+}$;*Braf*$^{V600E/+}$;*Pten*$^{flox/flox}$) orally treated by 6TG. We also ruled out the possibility that the enhanced tumor control was driven via the activation of immunogenic cell death by documenting that 6TG treatment of Yumm1.1 cells did not increase the expression of key ICD markers (cell surface expression of CRT and HMGB1 release)[33,45] . These results support our original hypothesis that the increase in TMB may increase the likelihood of neoantigen presentation on tumor cells which can, in turn, lead to increased and accelerated recruitment of T cells and improved tumor control. Whether the enhanced tumor control and immunogenicity are solely due to the increased TMB caused by 6TG or whether there are other mechanisms involved, requires further investigation.

Even though cancer immunotherapy based on PD-1/PD-L1 blockade has led to prolonged overall survival of many patients, a large proportion of cancer patients do not respond.[46,47] We assumed that the increased TMB and immunogenic immune infiltrates would enhance the efficacy of anti-PD1 treatment in the 6TG-YummTG1.1 group. Indeed, we identified a significant benefit in the 6TG-YummTG1.1 group receiving anti-PD1 with tumor volumes being smaller. Nevertheless, anti-PD1 treatment did not lead to complete inhibition of tumor growth, implying that potential immunosuppressive mechanisms were not fully abrogated. The presence of Ly6C$^{hi}$ myeloid cells, which were abundant in the 6TG-YummTG1.1 tumors, has previously been shown to hinder the efficacy of anti-PD1 therapy in non-small-cell lung carcinoma (NSCLC) patients.[48] Depleting Ly6C cells in a syngeneic lung adenocarcinoma mouse model improved antitumor efficacy of anti-PD1 therapy via expansion of effector CD8 T cells.[48] Furthermore, whereas anti-PD1 therapy improved tumor control in mice with 6TG-pretreated tumors, we did not observe the same effect when 6TG was administered orally to simulate a clinical context. This might be because of limitations strictly related to the preclinical animal model that prevented us from accurately mimicking the clinical situation. The short-term exposure to 6TG, for example, may have been insufficient to allow the full establishment of the negative interactions leading to the expression of PD1 and corresponding ligands, which would be a prerequisite for a more striking anti-PD1 treatment effect. Nevertheless, it is worth mentioning that, apart from anti-PD1, other immune-checkpoint inhibitors may be used (in combination or alone) to achieve tumor regression. The role of immunosuppressive cells and other inhibitory mechanisms in our experimental conditions warrant further investigation.

Other mouse models using Yumm1.7 cells have also studied the effect of TMB on antitumor immunity and ICI therapy success.[49,50] These models were based on the expansion of a single cell-derived clone with increased TMB. In our model, we induced random mutations every time we treated the Yumm1.1 cells with 6TG prior to injection. We hypothesize that these mutations, even though they were random, increased the neoantigen load. As a result, the likelihood of eliciting

weekly and the tumor kinetics was evaluated (n = 8–9). C) Tumor kinetics in mice receiving 600.000 CTRL-Yumm1.1 and being treated with anti-PD1/isotype starting one day following cell injections (n = 8). D) Tumor kinetics in mice receiving 600.000 6TG-YummTG1.1 and being treated with anti-PD1/isotype starting one day following cell injections (n = 9). Arrows represent anti-PD1/isotype injections. Data are representative of two independent experiments. Each data point corresponds to the mean tumor volume ± SD, as determined for each experimental group.

a potent antitumor T cell response is increased and the immunological control of tumor growth may be further improved by ICI therapy. Taking into consideration that every patient under thiopurine treatment might induce their own profile of mutations, we consider our model a valuable tool to draw conclusions of clinical relevance.

Overall, our data strongly indicate that 6TG-YummTG1.1 tumors are better controlled than CTRL-Yumm1.1 tumors due to differences in the adaptive immune response. We found 6TG-YummTG1.1 tumors to have distinct immune microenvironment and higher TMB. As a final point, the already better controlled 6TG-YummTG1.1 tumors were found responsive to anti-PD1 therapy, which serves as a proof-of-concept for the ongoing clinical trial testing the efficacy of combining the TEAM strategy with ICI therapy (NCT05276284).

## Acknowledgments

The authors acknowledge the staff of the Animal Facility at the Danish Cancer Society, the Histocore Facility at Copenhagen University, the Center for Genomic Medicine at Copenhagen University Hospital, and Laila Fischer for help with secretarial work. This project has received financial support from The Danish Ministry of Health (Sundhedsstyrelsen Grant no: 05-0400-45), The Danish Childhood Cancer Foundation (Børnecancerfonden 2019-5963, 2019-5934, 2020-5769). The work is part of the Danish nation-wide research program Childhood Oncology Network Targeting Research, Organisation & Life expectancy (CONTROL) and supported by the Danish Cancer Society (R204-A12424 to D.D.Z.; R-257-A14720 to K.S.). D.D.Z. is supported by the Melanoma Research Alliance (MRA 620385) and the LEO Foundation (LF-OC-19-000004). The Melanoma Research Team is part of the Center of Excellence for Autophagy, Recycling and Disease (CARD), funded by Danmarks Grundforskningsfond (DNRF125).

## Disclosure statement

The authors declare no potential conflicts of interests.

## Funding

This work was supported by the Børnecancerfonden [2019-5963]; Børnecancerfonden [2019-5934]; Børnecancerfonden [2020-5769]; Danmarks Grundforskningsfond [DNRF125]; LEO Fondet [LF-OC-19-000004]; Melanoma Research Alliance young investigator [MRA 620385]; Sundhedsstyrelsen [05-0400-45]; the Danish Cancer Society [R204-A12424]; the Danish Cancer Society [R-257-A14720].

## ORCID

Daniela De Zio http://orcid.org/0000-0002-9454-402X

## Data availability statement

The WGS and RNAseq datasets generated and analysed during the current study are currently deposited on Computerome, the Danish National Computer for Life Sciences, and will be available from the corresponding author on request. https://computerome.dtu.dk

## References

1. St Paul M, Ohashi PS. The Roles of CD8(+) T Cell Subsets in Antitumor Immunity. Trends Cell Biol. 2020;30:695–704. doi:10.1016/j.tcb.2020.06.003.
2. Tay RE, Richardson EK, Toh HC. Revisiting the role of CD4(+) T cells in cancer immunotherapy-new insights into old paradigms. Cancer Gene Ther. 2021;28:5–17. doi:10.1038/s41417-020-0183-x.
3. Waldman AD, Fritz JM, Lenardo MJ. A guide to cancer immunotherapy: from T cell basic science to clinical practice. Nat Rev Immunol. 2020;20:651–668.
4. Robert C. A decade of immune-checkpoint inhibitors in cancer therapy. Nat Commun. 2020;11:3801. doi:10.1038/s41467-020-17670-y.
5. Sharma P, Hu-Lieskovan S, Wargo JA, Ribas A. Primary, adaptive, and acquired resistance to cancer immunotherapy. Cell. 2017;168:707–723. doi:10.1016/j.cell.2017.01.017.
6. Jensen BA, Pedersen SR, Christensen JP, Thomsen AR, Bachmann MP. The availability of a functional tumor targeting T-cell repertoire determines the anti-tumor efficiency of combination therapy with anti-CTLA-4 and anti-4-1BB antibodies. PLoS One. 2013;8:e66081. doi:10.1371/journal.pone.0066081.
7. Jardim DL, Goodman A, de Melo Gagliato D, Kurzrock R. The challenges of tumor mutational burden as an immunotherapy biomarker. Cancer Cell. 2021;39:154–173. doi:10.1016/j.ccell.2020.10.001.
8. Anagnostou V, Bruhm, D. C., Niknafs, N., White, J. R., Shao, X. M., Sidhom, J. W. & Velculescu, V. E. Integrative tumor and immune cell multi-omic analyses predict response to immune checkpoint blockade in Melanoma. Cell Rep Med. 2020;1:100139. doi:10.1016/j.xcrm.2020.100139.
9. Lee M, Samstein RM, Valero C, Chan TA, Morris LGT. Tumor mutational burden as a predictive biomarker for checkpoint inhibitor immunotherapy. Hum Vaccin Immunother. 2020;16:112–115. doi:10.1080/21645515.2019.1631136.
10. Maleki Vareki S. High and low mutational burden tumors versus immunologically hot and cold tumors and response to immune checkpoint inhibitors. J Immunother Cancer. 2018;6:157. doi:10.1186/s40425-018-0479-7.
11. Litchfield K, Reading JL, Puttick C, Thakkar K, Abbosh C, Bentham R, Watkins TBK, Rosenthal R, Biswas D, Rowan A, *et al.* Meta-analysis of tumor- and T cell-intrinsic mechanisms of sensitization to checkpoint inhibition. Cell. 2021;184:596–614 e514. doi:10.1016/j.cell.2021.01.002.
12. Samstein RM, Lee C-H, Shoushtari AN, Hellmann MD, Shen R, Janjigian YY, Barron DA, Zehir A, Jordan EJ, Omuro A, *et al.* Tumor mutational load predicts survival after immunotherapy across multiple cancer types. Nat Genet. 2019;51:202–206. doi:10.1038/s41588-018-0312-8.
13. Karran P, Attard N. Thiopurines in current medical practice: molecular mechanisms and contributions to therapy-related cancer. Nat Rev Cancer. 2008;8:24–36. doi:10.1038/nrc2292.
14. Nielsen SN, Grell K, Nersting J, Abrahamsson J, Lund B, Kanerva J, Jónsson ÓG, Vaitkeviciene G, Pruunsild K, Hjalgrim LL, *et al.* DNA-thioguanine nucleotide concentration and relapse-free survival during maintenance therapy of childhood acute lymphoblastic leukaemia (NOPHO ALL2008): a prospective substudy of a phase 3 trial. Lancet Oncol. 2017;18:515–524. doi:10.1016/S1470-2045(17)30154-7.
15. Toksvang LN, Als-Nielsen B, Bacon C, Bertasiute R, Duarte X, Escherich G, Helgadottir EA, Johannsdottir IR, Jónsson ÓG, Kozlowski P, *et al.* Thiopurine Enhanced ALL Maintenance (TEAM): study protocol for a randomized study to evaluate the improvement in disease-free survival by adding very low dose 6-thioguanine to 6-mercaptopurine/methotrexate-based maintenance therapy in pediatric and adult patients (0-45 years) with newly diagnosed B-cell precursor or T-cell acute lymphoblastic leukemia treated according to the intermediate risk-high group of the ALLTogether1 protocol. BMC Cancer. 2022;22:483. doi:10.1186/s12885-022-09522-3.
16. Larsen RH, Utke Rank C, Grell K, Nørgaard Møller L, Malthe Overgaard U, Kampmann P, Nersting J, Degn M, Nygaard Nielsen S, Holst H, *et al.* Increments in DNA-thioguanine level during thiopurine-enhanced maintenance therapy of acute

lymphoblastic leukemia. Haematologica. 2021;106:2824–2833. doi:10.3324/haematol.2020.278166.
17. Meeth K, Wang JX, Micevic G, Damsky W, Bosenberg MW. The YUMM lines: a series of congenic mouse melanoma cell lines with defined genetic alterations. Pigment Cell Melanoma Res. 2016;29:590–597. doi:10.1111/pcmr.12498.
18. Homet Moreno B, Zaretsky JM, Garcia-Diaz A, Tsoi J, Parisi G, Robert L, Meeth K, Ndoye A, Bosenberg M, Weeraratna AT, *et al*. Response to programmed cell death-1 blockade in a murine Melanoma syngeneic model requires costimulation, CD4, and CD8 T cells. Cancer Immunol Res. 2016;4:845–857. doi:10.1158/2326-6066.CIR-16-0060.
19. Di Leo L, Bodemeyer V, Bosisio FM, Claps G, Carretta M, Rizza S, Faienza F, Frias A, Khan S, Bordi M, *et al*. Loss of Ambra1 promotes melanoma growth and invasion. Nat Commun. 2021;12:2550. doi:10.1038/s41467-021-22772-2.
20. Jacobsen JH, Schmiegelow K, Nersting J. Liquid chromatography-tandem mass spectrometry quantification of 6-thioguanine in DNA using endogenous guanine as internal standard. J Chromatogr B Analyt Technol Biomed Life Sci. 2012;881-882:115–118. doi:10.1016/j.jchromb.2011.11.032.
21. Shipkova M, Armstrong VW, Wieland E, Oellerich M. Differences in nucleotide hydrolysis contribute to the differences between erythrocyte 6-thioguanine nucleotide concentrations determined by two widely used methods. Clin Chem. 2003;49:260–268. doi:10.1373/49.2.260.
22. Li H, Durbin R. Fast and accurate long-read alignment with Burrows-Wheeler transform. Bioinformatics. 2010;26:589–595. doi:10.1093/bioinformatics/btp698.
23. McKenna A, Hanna M, Banks E, Sivachenko A, Cibulskis K, Kernytsky A, Garimella K, Altshuler D, Gabriel S, Daly M, *et al*. The genome analysis toolkit: a mapreduce framework for analyzing next-generation DNA sequencing data. Genome Res. 2010;20:1297–1303. doi:10.1101/gr.107524.110.
24. Cibulskis K, Lawrence MS, Carter SL, Sivachenko A, Jaffe D, Sougnez C, Gabriel S, Meyerson M, Lander ES, Getz G, *et al*. Sensitive detection of somatic point mutations in impure and heterogeneous cancer samples. Nat Biotechnol. 2013;31:213–219. doi:10.1038/nbt.2514.
25. Wang K, Li M, Hakonarson H. ANNOVAR: functional annotation of genetic variants from high-throughput sequencing data. Nucleic Acids Res. 2010;38:e164. doi:10.1093/nar/gkq603.
26. Mayakonda A, Lin DC, Assenov Y, Plass C, Koeffler HP. Maftools: efficient and comprehensive analysis of somatic variants in cancer. Genome Res. 2018;28:1747–1756. doi:10.1101/gr.239244.118.
27. Dobin A, Davis CA, Schlesinger F, Drenkow J, Zaleski C, Jha S, Batut P, Chaisson M, Gingeras TR. STAR: ultrafast universal RNA-seq aligner. Bioinformatics. 2013;29:15–21. doi:10.1093/bioinformatics/bts635.
28. Love MI, Huber W, Anders S. Moderated estimation of fold change and dispersion for RNA-seq data with DESeq2. Genome Biol. 2014;15:550. doi:10.1186/s13059-014-0550-8.
29. Subramanian A, Tamayo P, Mootha VK, Mukherjee S, Ebert BL, Gillette MA, Paulovich A, Pomeroy SL, Golub TR, Lander ES, *et al*. Gene set enrichment analysis: a knowledge-based approach for interpreting genome-wide expression profiles. Proc Natl Acad Sci U S A. 2005;102:15545–15550. doi:10.1073/pnas.0506580102.
30. Monteiro LB, Davanzo GG, de Aguiar CF, Moraes-Vieira PMM. Using flow cytometry for mitochondrial assays. MethodsX. 2020;7:100938. doi:10.1016/j.mex.2020.100938.
31. Toksvang LN, Grell K, Nielsen SN, Nersting J, Murdy D, Moorman AV, Vora A, Schmiegelow K. DNA-TG and risk of sinusoidal obstruction syndrome in childhood acute lymphoblastic leukemia. Leukemia. 2022;36:555–557. doi:10.1038/s41375-021-01420-0.
32. Toksvang LN, Grell K, Nersting J, Degn M, Nielsen SN, Abrahamsson J, Lund B, Kanerva J, Jónsson ÓG, Lepik K, *et al*. DNA-thioguanine concentration and relapse risk in children and young adults with acute lymphoblastic leukemia: an IPD meta-analysis. Leukemia. 2022;36:33–41. doi:10.1038/s41375-021-01182-9.
33. Fucikova J, Kepp, O., Kasikova, L., Petroni, G., Yamazaki, T., Liu, P., & Galluzzi, L. Detection of immunogenic cell death and its relevance for cancer therapy. Cell Death Dis. 2020;11:1013. doi:10.1038/s41419-020-03221-2.
34. Wang P, Chen Y, Wang C. Beyond tumor mutation burden: tumor neoantigen burden as a biomarker for immunotherapy and other types of therapy. Front Oncol. 2021;11:672677. doi:10.3389/fonc.2021.672677.
35. Fujimura T, Kambayashi Y, Aiba S. Crosstalk between regulatory T cells (Tregs) and myeloid derived suppressor cells (MDSCs) during melanoma growth. Oncoimmunology. 2012;1:1433–1434. doi:10.4161/onci.21176.
36. Brinkmann V, Davis MD, Heise CE, Albert R, Cottens S, Hof R, Bruns C, Prieschl E, Baumruker T, Hiestand P, *et al*. The immune modulator FTY720 targets sphingosine 1-phosphate receptors. J Biol Chem. 2002;277:21453–21457. doi:10.1074/jbc.C200176200.
37. Baeyens A, Fang V, Chen C, Schwab SR. Exit Strategies: S1P Signaling and T Cell Migration. Trends Immunol. 2015;36:778–787. doi:10.1016/j.it.2015.10.005.
38. Lelliott EJ, Cullinane, C., Martin, C. A., Walker, R., Ramsbottom, K. M., Souza-Fonseca-Guimaraes, F., & Sheppard, K. E. A novel immunogenic mouse model of melanoma for the preclinical assessment of combination targeted and immune-based therapy. Sci Rep. 2019;9:1225.
39. Salas-Benito D, Pérez-Gracia JL, Ponz-Sarvisé M, Rodriguez-Ruiz ME, Martínez-Forero I, Castañón E, López-Picazo JM, Sanmamed MF, Melero I. Paradigms on immunotherapy combinations with chemotherapy. Cancer Discov. 2021;11:1353–1367. doi:10.1158/2159-8290.CD-20-1312.
40. Kat A, Thilly WG, Fang WH, Longley MJ, Li GM, Modrich P. An alkylation-tolerant, mutator human cell line is deficient in strand-specific mismatch repair. Proc Natl Acad Sci U S A. 1993;90:6424–6428. doi:10.1073/pnas.90.14.6424.
41. Branch P, Aquilina G, Bignami M, Karran P. Defective mismatch binding and a mutator phenotype in cells tolerant to DNA damage. Nature. 1993;362:652–654. doi:10.1038/362652a0.
42. Zheng M. Tumor mutation burden for predicting immune checkpoint blockade response: the more, the better. J Immunother Cancer. 2022;10:e003087. doi:10.1136/jitc-2021-003087.
43. Zou XL, Li X-B, Ke H, Zhang G-Y, Tang Q, Yuan J, Zhou C-J, Zhang J-L, Zhang R, Chen W-Y, *et al*. Prognostic value of neoantigen load in immune checkpoint inhibitor therapy for cancer. Front Immunol. 2021;12:689076. doi:10.3389/fimmu.2021.689076.
44. Beatty GL, Gladney WL. Immune escape mechanisms as a guide for cancer immunotherapy. Clin Cancer Res. 2015;21:687–692. doi:10.1158/1078-0432.CCR-14-1860.
45. Kroemer G, Galluzzi L, Kepp O, Zitvogel L. Immunogenic cell death in cancer therapy. Annu Rev Immunol. 2013;31:51–72. doi:10.1146/annurev-immunol-032712-100008.
46. Chamoto K, Hatae R, Honjo T. Current issues and perspectives in PD-1 blockade cancer immunotherapy. Int J Clin Oncol. 2020;25:790–800. doi:10.1007/s10147-019-01588-7.
47. Lei Q, Wang D, Sun K, Wang L, Zhang Y. Resistance mechanisms of anti-PD1/PDL1 therapy in solid tumors. Front Cell Dev Biol. 2020;8:672. doi:10.3389/fcell.2020.00672.
48. Feng J, Chen S, Li S, Wu B, Lu J, Tan L, Li J, Song Y, Shi G, Shi YG, *et al*. The association between monocytic myeloid-derived suppressor cells levels and the anti-tumor efficacy of anti-PD-1 therapy in NSCLC patients. Transl Oncol. 2020;13:100865. doi:10.1016/j.tranon.2020.100865.
49. Wang J, Perry CJ, Meeth K, Thakral D, Damsky W, Micevic G, Kaech S, Blenman K, Bosenberg M. UV-induced somatic mutations elicit a functional T cell response in the YUMMER1.7 mouse melanoma model. Pigment Cell Melanoma Res. 2017;30:428–435. doi:10.1111/pcmr.12591.
50. Gorgun FM, Widen SG, Tyler DS, Englander EW. Enhanced antitumor response to immune checkpoint blockade exerted by cisplatin-induced mutagenesis in a murine melanoma model. Front Oncol. 2021;11:701968. doi:10.3389/fonc.2021.701968.